

Optical investigation of electrical spin injection into semiconductorsV. F. Motsnyi,* P. Van Dorpe,† and W. Van Roy
*IMEC, Kapeldreef 75, B-3001 Leuven, Belgium*E. Goovaerts
*University of Antwerpen-UIA, Universiteitsplein 1, B-2610 Antwerpen, Belgium*V. I. Safarov
*GPEC, Département de Physique, Faculté des Sciences de Luminy, 13288 Marseille, France*G. Borghs and J. De Boeck
IMEC, Kapeldreef 75, B-3001 Leuven, Belgium
(Received 22 May 2003; published 24 December 2003)

We investigate the electrical injection of spin-polarized electrons into a semiconductor [Al(GaAs)] heterostructure from ferromagnetic FeCo metal through an AlO_x tunnel barrier. We have developed the optical oblique Hanle effect approach for the quantitative analysis of electrical spin injection into semiconductors. This technique is based on the manipulation of the electron spins within a semiconductor when spin polarized electrons have been injected. This allows us to clearly separate the effects caused by spin injection from others, that are magneto-optical, Zeeman, etc. Simultaneously, the oblique Hanle effect approach provides additional information on the spin dynamics in the semiconductor. In the FeCo/ AlO_x /Al(GaAs) heterostructures we observe spin injection of 21% and 16% at 80 and 300 K, respectively. The importance of electron thermalization effects and the impact of the doping level of the semiconductor for practical investigation of spin injection by optical means are demonstrated.

DOI: 10.1103/PhysRevB.68.245319

PACS number(s): 73.43.Jn, 73.61.Ey, 72.25.Hg, 75.50.Bb

I. INTRODUCTION

It is generally accepted that in the near future electronic device dimensions are going approach physical limits.¹ In the rapidly evolving field of spintronics, the electron spin is used as an additional degree of freedom to engineer devices with a higher performance with regards to power consumption and functionality, and as an enabler of new architectures.²⁻⁴ Here, the quantum mechanical concept of electron spin brings an amazing new functionality into the mainstream of charge based electronics. Following the success of magnetic multilayers and magnetic tunnel junctions⁵ the use of electron spin in semiconductor-based devices has received increasing attention.⁶ The established approach of creating a spin polarized electron ensemble in III-V semiconductors by means of circularly polarized light⁷ has revealed that the electron spin can have a long lifetime,^{8,9} and significant drift length,^{10,11} and can traverse the interfaces of two semiconductors with different g factors.¹² The most important principle for spintronic device implementation is the efficient electrical injection of spin polarized charges into a semiconductor from a magnetic contact, the so-called spin injection. For a long time the ability to efficiently inject spins into semiconductors remained an open question.¹³⁻¹⁷ It was shown that magnetic semiconductors, like paramagnetic BeMnZnSe (Ref. 18) and ferromagnetic GaMnAs,¹⁹ could be used to inject spins into semiconductors at low temperatures and, in the first case, by the application of a large magnetic field. Compared to the magnetic semiconductors, ferromagnetic metals (FMs) have significant advantages as materials for spintronic applications. These metals have a very large spin polarization even at room temperature and, moreover,

their physical properties and the fabrication technology are well known. Even though the electrical injection of spin-polarized electrons into a semiconductor from a ferromagnetic scanning tunneling tip was demonstrated,^{20,21} this approach is not practical for device implementation. Recently, spin injection in FM/semiconductor Schottky barriers²²⁻²⁴ and FM/oxide/semiconductor tunnel junction²⁵⁻²⁸ heterostructures were reported. In all these spin injection devices, often called spin light emitting diodes (spin LEDs), an optical technique (circular polarization of emitted light⁷) was used for the assessment of the injected spin polarization.

Typically these types of experiments are performed in a strong magnetic field applied perpendicularly to the FM surface leading to the number of the side effects (magneto-optical, Zeeman, etc.) masking the actual spin injection signal. In the following sections we show how the application of a small oblique magnetic field enables one to manipulate spins inside of a semiconductor, assess the spin injection, and separate the spin injection from the side effects. Furthermore we demonstrate our realization of spin LEDs and show their spin injection performance at low and room temperatures.

II. ELECTRON SPIN MANIPULATION IN THE SEMICONDUCTOR, FERROMAGNETIC FILM AND RELATED PHENOMENA

The idea of using light for spin injection and detection is not new and dates the late 1960s.²⁹ Later it was shown that conversion of the angular momentum of light into electron spin and vice versa is very efficient in III-V semiconductors.⁷ In these materials and in GaAs in particular, the absorption of 100% circularly polarized light leads, due to the selection

rules for transition probabilities, to the creation of an ensemble of electrons with preferential spin orientation along the axis of the light propagation $\Pi = 0.5$. Here Π is the degree of spin polarization of the electron ensemble $\Pi = (n^\uparrow - n^\downarrow)/(n^\uparrow + n^\downarrow)$, and n^\uparrow and n^\downarrow are numbers of spin-up and spin-down electrons.

In the radiative recombination process, due to the same selection rules of the transition probabilities, light of circular polarization $P = 1/2 \cdot \Pi$ is emitted along the axis of spin polarization of the electron ensemble. Where $P = (I^+ - I^-)/(I^+ + I^-)$ is the degree of circular polarization of light, and I^+ and I^- are the intensities of right and left circularly polarized components of light.

Under electrical spin injection into a semiconductor the observed emission of circular polarization is in fact the result of a multistep process. Generally at first, the spin-polarized electrons are injected into the conduction band of the semiconductor for the case where the kinetic energy is higher than $k \cdot T$ (hot electrons). Second, in the thermalization process and during the electron lifetime at the bottom of the conduction band, before recombination with holes, some loss of spin polarization may occur due to spin scattering. As a result, the measured steady state polarization can be significantly smaller than the originally injected one.

Further, due to the high refractive index of GaAs ($n_{\text{GaAs}} = 3.4$), only photons emitted within a small angle close to the sample surface normal can escape the solid state. But for most of the thin ferromagnetic films used in spintronic applications (Fe, Co, Ni, etc.) the magnetization orientation is in plane, as determined by the shape anisotropy. Hence, under radiative recombination of spin-polarized electrons injected from the thin ferromagnetic film into the semiconductor, the light emitted in the direction normal to the surface of the ferromagnetic film (and hence to the magnetization) is unpolarized. In order to optically assess the spin polarization, the spins must be manipulated (in the ferromagnetic film or within the semiconductor) in a way to obtain a non-zero component of the electron spin normal to the surface. One of the common solutions used consists of applying a strong magnetic field (more than 1 T for most common ferromagnetic thin films) perpendicular to the surface, that changes the magnetization of the ferromagnetic film and hence the orientation of the injected spins. This leads to side effects (Zeeman, magneto-optical, etc.) that scale with the external magnetic field or with the out-of-plane magnetization of the ferromagnetic film, complicating the quantitative assessment of electrical spin injection. Moreover, these side effects can dominate the measured quantities and even be entirely responsible for the observed dependencies.

We have developed an approach based on the oblique Hanle effect (first used for detection of nuclear spin polarization³⁰), where the application of a small oblique magnetic field enables one to manipulate spins inside of a semiconductor and assess spin injection without considerable change of the magnetization of the ferromagnetic layer. In addition, this technique reveals the spin dynamics inside the semiconductor simultaneously, separates the spin injection from the side effects and clearly demonstrates the nature of the observed effects.

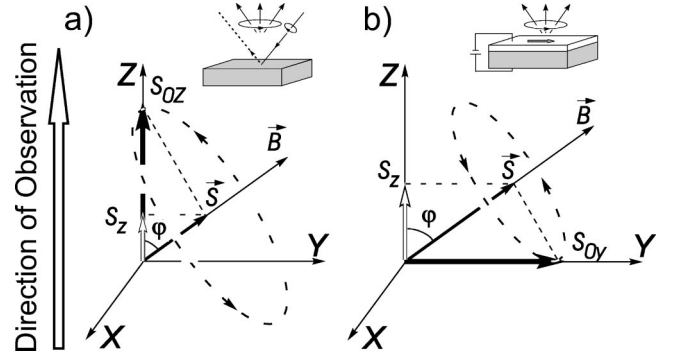


FIG. 1. Spin precession in the oblique magnetic field in the case of (a) optical spin injection and (b) electrical spin injection. Under steady state conditions the spin precession leads to averaging and vanishing of the component of \vec{S} perpendicular to \vec{B} . The remaining component is parallel to \vec{B} , and is accessible in measurements.

A. Hanle effect in an oblique magnetic field

In the solid state, the spin of an electron ensemble is characterized by the average electron spin $\vec{S} = \sum_i^n \vec{s}_i / n$, where \vec{s}_i is the spin of an individual electron and n is the number of electrons. The degree of spin polarization Π along \vec{S} is $\Pi = 2 \cdot |\vec{S}|$. Upon application of the magnetic field \vec{B} ($|\vec{B} \times \vec{S}| \neq 0$) the electron spins start to precess around \vec{B} with the Larmor frequency $\vec{\Omega} = (g^* \cdot \mu_B / \hbar) \cdot \vec{B}$, where g^* is the effective g factor and μ_B is the Bohr magneton.

Within the semiconductor, the evolution of the average electron spin \vec{S} , taking into account spin injection, spin scattering and electron recombination processes, is described by the Bloch-type equation⁷

$$\frac{d\vec{S}}{dt} = \frac{\vec{S}_0}{\tau} - \frac{\vec{S}}{T_s} + [\vec{\Omega} \times \vec{S}], \quad (1)$$

where \vec{S}_0 is the average injected electron spin, τ is the lifetime of the electrons (i.e., electron recombination time), and T_s is the spin lifetime ($T_s^{-1} = \tau^{-1} + \tau_s^{-1}$, where τ_s is the spin scattering time).

In steady state conditions ($d\vec{S}/dt = 0$), this equation has very simple solutions. In the geometry of the experimental configuration depicted in Fig. 1, the XY plane is the sample plane, the OZ axis is pointing along the direction of observation and the OY axis coincides with the easy axis of ferromagnetic film magnetization. The external oblique magnetic field $\vec{B}(0, B_y, B_z)$ is applied under an angle φ to the OZ axis. Below we present the magnetic field dependencies only for the S_z component of the average electron spin \vec{S} , since only this component can be detected optically.

In the case of optical spin injection using circularly polarized light $\vec{S}_0(0, 0, S_{0z})$, the solution of Eq. (1) for the S_z component is

$$\begin{aligned} S_z &= S_{0z} \cdot \frac{T_s}{\tau} \cdot \frac{1 + (\Omega \cdot T_s)^2 \cdot \cos^2 \varphi}{1 + (\Omega \cdot T_s)^2} \\ &= S_{0z} \cdot \frac{T_s}{\tau} \cdot \frac{1 + (B/\Delta B)^2 \cdot \cos^2 \varphi}{1 + (B/\Delta B)^2}, \end{aligned} \quad (2)$$

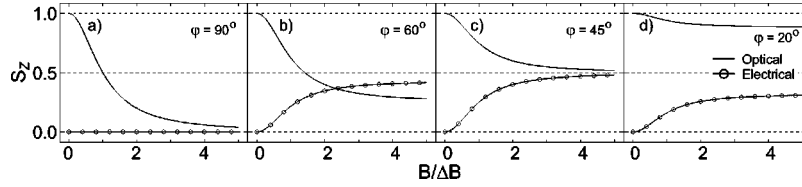


FIG. 2. The S_z component of the average electron spin \vec{S} (normalized to $S_0 \cdot T_s / \tau$), in the case of optical $\vec{S}_0(0,0,S_{0z})$ and electrical $\vec{S}_0(0,S_{0Y},0)$ spin injection into a semiconductor in the oblique Hanle effect geometry [Fig. 1, $\vec{B}(0,B_Y,B_z)$] for different oblique angles φ , as given by Eqs. (2) and (4). The magnetic field is expressed in units of $\Delta B = [(g^* \cdot \mu_B / \hbar) \cdot T_s]^{-1}$, the half-width of the Hanle curve.

where

$$\Delta B = \left(\frac{g^* \cdot \mu_B}{\hbar} \cdot T_s \right)^{-1} \quad (3)$$

is the Hanle curve half-width, corresponding to the condition $\Omega \cdot T_s = 1$.

In the case of electrical spin injection $\vec{S}_0(0,S_{0Y},0)$ the dependency of S_z as a function of the external magnetic field is different:

$$\begin{aligned} S_z &= S_{0Y} \cdot \frac{T_s}{\tau} \cdot \frac{(\Omega \cdot T_s)^2 \cdot \cos \varphi \cdot \sin \varphi}{1 + (\Omega \cdot T_s)^2} \\ &= S_{0Y} \cdot \frac{T_s}{\tau} \cdot \frac{(B/\Delta B)^2 \cdot \cos \varphi \cdot \sin \varphi}{1 + (B/\Delta B)^2}. \end{aligned} \quad (4)$$

The magnetic field dependencies of S_z (normalized to $S_0 \cdot T_s / \tau$) for electrical and optical spin injection, after Eqs. (2) and (4), are presented in Fig. 2 for different oblique angles φ .

In the case of optical spin injection $\vec{S}_0(0,0,S_{0z})$, the S_z component of the average electron spin \vec{S} has a maximum at $B=0$ and decreases with the application of a magnetic field. The $S_z(B)$ dependency has a Lorentzian shape; the value of the asymptotical minimum depends on the angle φ , and is zero at $\varphi=90^\circ$ (ordinary Hanle effect).

The surprising fact that S_z is nonzero in the case of electrical spin injection from the in-plane magnetized ferromagnetic film $\vec{S}_0(0,S_{0Y},0)$ has interesting consequences for an optical investigation of electrical spin injection into semiconductors. S_z grows from zero at $B=0$ and saturates at higher values of external magnetic field $B \gg \Delta B$. The curve is strongly non-linear. The half-width ΔB (corresponding again to the condition $\Omega \cdot T_s = 1$) is determined by the effective g factor and spin lifetime T_s within the semiconductor. This provides a unique signature of spin injection compared to the

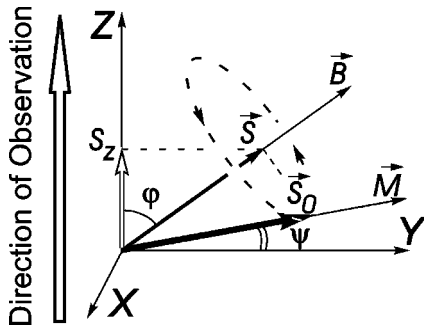


FIG. 3. Tilting of the magnetization \vec{M} of the thin ferromagnetic film under application of the oblique magnetic field $\vec{B}(0,B_Y,B_z)$ in the oblique Hanle effect experimental configuration.

side effects, which are linear or nearly linear with external magnetic field.

The S_z saturation value is dependent on the angle φ , having maximum of $S_{z \text{ MAX}} = 1/2 \cdot S_{0Y} \cdot T_s / \tau$ for $\varphi = 45^\circ$. Thus the S_z value measured from the polarization P of the luminescence ($S_z = P$) at saturation is lower than the injected one S_{0Y} by the factor $1/2 \cdot T_s / \tau$, and the degree of injected spin polarization Π is related to the measured degree of circular polarization of light at saturation for $\varphi = 45^\circ$ as

$$\Pi = 2 \cdot S_{0Y} = 4 \cdot S_{z \text{ MAX}} \cdot \tau / T_s = 4 \cdot P_{\text{Sat}} \cdot \tau / T_s. \quad (5)$$

The parameter T_s / τ describes the spin scattering of the electrons during their lifetime on the bottom of the conduction band of the semiconductor and can be measured in the complete optical experiment under excitation with 100% circularly polarized light, when the injected spin polarization is perfectly known $\vec{S}_0(0,0,1/4)$.⁷

However, the optical assessment of electrical spin injection in a real device implies consideration of some other side effects. Below we show how one can take into account the influence of tilting (rotation) of the ferromagnetic film magnetization in the small external oblique magnetic field, the magneto-optical effects caused by the ferromagnetic film and the influence of electron thermalization processes in the semiconductor.

B. Tilting of the ferromagnetic film magnetization in the oblique magnetic field

An oblique magnetic field applied under angle φ with the magnetization axis of a ferromagnetic film (OZ axis) will force the magnetization to tilt (rotate) out of plane by an angle ψ (Fig. 3). This will lead to the spin injection $\vec{S}_0(0,S_{0Y}^*,S_{0z}^*)$, which is different from the case described in Sec. II A.

Starting from Eq. (1), for the same applied oblique magnetic field $\vec{B}(0,B_Y,B_z)$ one can easily obtain an expression for the S_z component of the average electron spin \vec{S} :

$$\begin{aligned} S_z &= S_{0Y}^* \cdot \frac{T_s}{\tau} \cdot \frac{(\Omega \cdot T_s)^2 \cdot \cos \varphi \cdot \sin \varphi}{1 + (\Omega \cdot T_s)^2} \\ &\quad + S_{0z}^* \cdot \frac{T_s}{\tau} \cdot \frac{1 + (\Omega \cdot T_s)^2 \cdot \cos^2 \varphi}{1 + (\Omega \cdot T_s)^2} \\ &= S_{0Y}^* \cdot \frac{T_s}{\tau} \cdot \frac{(B/\Delta B)^2 \cdot \cos \varphi \cdot \sin \varphi}{1 + (B/\Delta B)^2} \\ &\quad + S_{0z}^* \cdot \frac{T_s}{\tau} \cdot \frac{1 + (B/\Delta B)^2 \cdot \cos^2 \varphi}{1 + (B/\Delta B)^2}, \end{aligned} \quad (6)$$

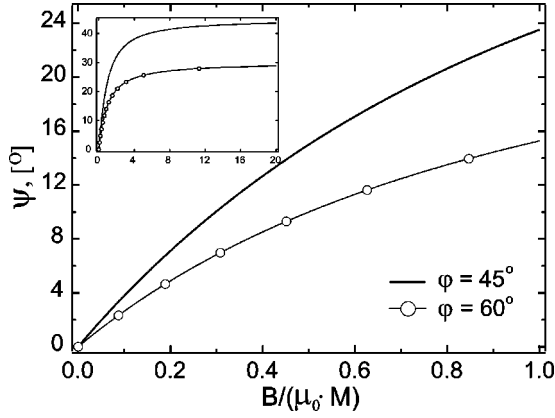


FIG. 4. The tilting angle ψ as a function of the $B/(\mu_0 \cdot M)$ ratio for different oblique angles $\varphi=45^\circ$ and 60° , after Eq. (8) (inset extended field range).

where $S_{0Y}^* = S_0 \cdot \cos \psi$ and $S_{0z}^* = S_0 \cdot \sin \psi$. Now S_z has two components identical to Eqs. (2) and (4) with amplitudes which are functions of the tilting angle ψ . The magnitude of the angle ψ is dependent on the film saturation magnetization M , angle φ and magnitude of the external applied field $H_{ext} = B/\mu_0$.

For the calculation of the tilting angle ψ we make the following considerations. The shape anisotropy energy (or demagnetization energy) density is given by $U_d = -\mu_0 \cdot (\vec{M} \cdot \vec{H}_d)/2$, where $\vec{H}_d = -\vec{M}_z$ is the demagnetizing field and M_z is the out-of-plane magnetization of the film. The total energy density of the film in an external field \vec{H}_{ext} is then given by

$$U = -\mu_0 \cdot (\vec{M} \cdot \vec{H}_{ext}) - \frac{\mu_0 \cdot (\vec{M} \cdot \vec{H}_d)}{2} \\ = -\mu_0 \cdot M \cdot H_{ext} \cdot \sin(\varphi + \psi) + \frac{\mu_0 \cdot M^2}{2} \cdot \sin^2 \psi, \quad (7)$$

and the minimum is obtained for the tilt angle ψ given by

$$\frac{B}{\mu_0 \cdot M} = \frac{\sin \psi \cdot \cos \psi}{\cos \varphi \cdot \cos \psi - \sin \varphi \cdot \sin \psi}. \quad (8)$$

The dependencies of the tilting angle ψ on the external oblique magnetic field \vec{B} , taken after Eq. (8), are shown in Fig. 4 for two different field angles $\varphi=45^\circ$ and $\varphi=60^\circ$. The angle ψ has an almost linear dependency at small values of B with saturation at higher values. The saturation value is $\psi = 90^\circ - \varphi$.

Note that the angle ψ is dependent on the magnetic field B thus the S_{0Y}^* and S_{0z}^* components of the average electron spin also depend on B . This leads to deformation of the Hanle curves described in Sec. II A. Figure 5 shows the calculated dependencies of $S_z(B)$ resulting from Eqs. (6), (8), and (4) for oblique angle $\varphi=45^\circ$. The important parameter is the ratio between the half-width of the Hanle curve ΔB and the saturation magnetization $\mu_0 \cdot M$ of the film. Figure 5(a) shows the $S_z(B)$ dependency described by Eqs. (6) and (8)

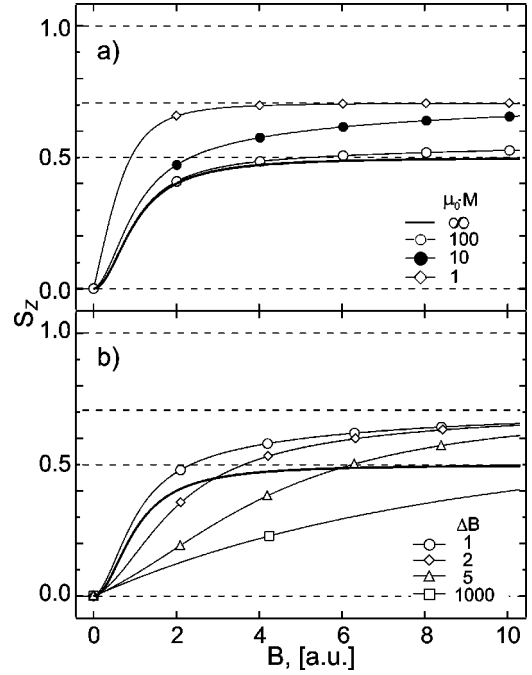


FIG. 5. The S_z component of the average electron spin \vec{S} (normalized to $S_0 \cdot T_s / \tau$) as a function of the oblique magnetic field \vec{B} ($\varphi=45^\circ$) for different $\Delta B/(\mu_0 \cdot M)$ ratios after Eqs. (6), (8), and (4). (a) The $S_z(B)$ dependency for different ferromagnetic materials and different values of saturation magnetization $\mu_0 \cdot M$, while $\Delta B = 1$ is fixed. (b) The $S_z(B)$ dependency for different semiconductor spin detectors—different half-width of Hanle curve $\Delta B = [(g^* \cdot \mu_B / \hbar) \cdot T_s]^{-1}$, while $\mu_0 \cdot M = 10$ is fixed. The bold line corresponds to the $S_z(B)$ dependency for in-plane spin injection $\vec{S}_0(0, S_{0Y}, 0)$ [Eq. (4)], when $\Delta B = 1$. The values of B , ΔB , and $\mu_0 \cdot M$ are expressed in the same arbitrary units.

for various values of the $\mu_0 \cdot M$, while ΔB is fixed at $\Delta B = 1$. Figure 5(b) shows the opposite case, when the $\mu_0 \cdot M$ is fixed and the ΔB takes different values. (A change of ΔB can be achieved by changing the temperature as well as semiconductor heterostructure, doping level, etc.⁷) The bold line represents $S_z(B)$ without taking into account the tilting of magnetization in ferromagnetic film [Eq. (4)]. One can see that the change of the S_z caused by the tilting of the ferromagnetic film magnetization in the oblique magnetic field indeed depends on the $\Delta B/(\mu_0 \cdot M)$ ratio, and in the general case cannot be neglected. This contribution can be easily taken into account in the fitting of experimental data, when the saturation magnetization of the thin ferromagnetic film is known from independent measurements.

This correction in the fitting procedure decreases the values of ΔB and Π . However, the experience shows (see Sec. IV A) that for our FeCo/AlO_x/Al(GaAs) MIS spin LEDs this correction does not exceed 10% and 20% of the values of ΔB and Π , respectively, obtained from the fitting without taking into account the tilting effect. (In our case, the ferromagnetic film saturation magnetization is $\mu_0 \cdot M = 1.3T$ and the external magnetic field does not exceed $B \leq 0.6T$, see Secs. III–IV.)

C. Influence of magneto-optical effects

In the surface emitting spin LED the light emitted in the semiconductor propagates through the thin semi-transparent ferromagnetic layer, which has some out-of-plane magnetization caused by the tilting of the magnetization in the external oblique magnetic field. So the magneto-optical circular dichroism (MCD), i.e., the difference in absorption of the light with left and right circular polarization by the ferromagnetic film, can influence the resulting degree of circular polarization. This effect can be easily taken into account.

The MCD contribution to the polarization of the light can be characterized by $D = (T^+ - T^-)/(T^+ + T^-) = \Delta T/T$, where $T^+ = T + \Delta T$ and $T^- = T - \Delta T$ are transmissions of right and left circular polarization components of light in the ferromagnetic film (as result of different absorption). The intensities of right and left circular polarization components of light emitted as a result of the recombination of a spin polarized electron ensemble inside the semiconductor can be expressed as $I^+ = I + \Delta I$ and $I^- = I - \Delta I$. And the degree of circular polarization is then $P_{inj} = (I^+ - I^-)/(I^+ + I^-) = \Delta I/I$. The resulting intensities of right and left circular polarization components of light after propagation through the ferromagnetic film are $I_{meas}^+ = T^+ \cdot I^+$, $I_{meas}^- = T^- \cdot I^-$. So the measured degree of circular polarization of light is

$$P_{meas} = \frac{I_{meas}^+ - I_{meas}^-}{I_{meas}^+ + I_{meas}^-} = \frac{\Delta T}{T} \cdot \left(1 - \frac{\Delta T}{T} \cdot \frac{\Delta I}{I} \right) + \frac{\Delta I}{I} \cdot \left(1 - \frac{\Delta T}{T} \cdot \frac{\Delta I}{I} \right). \quad (9)$$

For typical real structures one generally has $\Delta T/T \ll 1$ and $\Delta I/I \ll 1$ ($\Delta T/T \approx 10^{-3}$, $\Delta I/I \approx 10^{-1} \dots 10^{-3}$), so the experimentally measured degree of circular polarization can be represented just as

$$P_{meas} \approx P_{inj} + D. \quad (10)$$

The contribution of MCD to the resulting circular polarization of the emitted light can be quantitatively characterized in a simple photoluminescence experiment. Excitation with unpolarized or linearly polarized light creates in the semiconductor the population of unpolarized electrons.⁷ Their radiative recombination with holes results in emission of the unpolarized light with $P_{inj} = 0$. Thus, from Eq. (10) the measurement of circular polarization of photoluminescence under such excitation provides directly the D value, which characterizes the MCD effect in the ferromagnetic film.

In the same experiment one can also take into account the polarization of luminescence due to Zeeman splitting of electron spin states in the external magnetic field.^{31,7} As shown below this effect is very weak, and can be neglected practically in all measurements.

In semiconductor under thermal equilibrium the population of spin-up and spin-down states, splitted by external magnetic field, is given by Boltzmann statistics

$$\frac{n^\uparrow}{n^\downarrow} = \exp\left(-\frac{g^* \cdot \mu_B \cdot B}{k \cdot T}\right).$$

The average electron spin \vec{S} corresponding to Zeeman splitting, which is inferior to the thermal energy (it is always the case in our experiments), is given by the following expression:

$$S_{Zeeman} = \frac{1}{2} \cdot \frac{n^\uparrow - n^\downarrow}{n^\uparrow + n^\downarrow} \approx \frac{1}{4} \cdot \frac{g^* \cdot \mu_B \cdot B}{k \cdot T}. \quad (11)$$

Since the lifetime of electrons being optically or electrically injected into semiconductor is comparable to their spin relaxation time, the injected electrons cannot reach the complete thermal equilibrium and Eq. (11) has to be weighted by the factor T_s/τ_s that is always inferior to the unity. In this case the corresponding polarization of luminescence in the direction of observation can be expressed in the following way:

$$P_{Zeeman} = S_{Zeeman} \cdot \frac{T_s}{\tau_s} \cdot \cos \varphi. \quad (12)$$

In the case of GaAs, the estimations for the electron Zeeman splitting contribution to the circular polarization of luminescence at 80 K gives $P_{Zeeman} \approx 10^{-4}$ in the highest field used in our experiments. This contribution, which is also a linear function of B , can be easily measured in the simple experiment under optical excitation with linearly polarized light, exactly the same way as in the case with MCD. Hence, the measurements of D described above include all magneto-optical effects, the MCD in ferromagnetic film and Zeeman splitting in semiconductor.

D. Electron thermalization in the semiconductor

In the semiconductor heterostructure under application of sufficiently high bias, the hot electrons are injected into the active region of a spin LED [Fig. 6(a)]. It can happen that during their thermalization to the bottom of the conduction band these electrons lose their spin orientation. This effect was studied in detail in all-optical experiments^{32,7} in the 1970s. The loss of spin polarization during the thermalization process depends on the speed of electron thermalization, which is different for the samples with different doping levels. In highly doped samples the thermalization is rapid and polarization losses are small and even insignificant. In low-doped samples the thermalization process is slow and spin losses during thermalization could be high. Clear indication on the role of thermalization can be obtained from the all-optical experiments with different wavelengths of the exciting light.

For the exciting photon energy [Fig. 6(b)] exceeding $E_g + \Delta$, where Δ is the spin orbit splitting of the valence band, the spin polarization of the photoexcited electrons is strongly reduced, due to the fact that electrons excited from the split-off band have opposite spin orientations as compared to the electrons excited from the upper bands of the light and heavy holes.^{32,7} In the general case, the contribution of the latter ones prevails and the net spin polarization stays positive, but reduced in value. However, the electrons excited from the upper valence bands have much higher kinetic energy and should be thermalized to the bottom of the conduction band before recombination takes place. If these hot electrons even

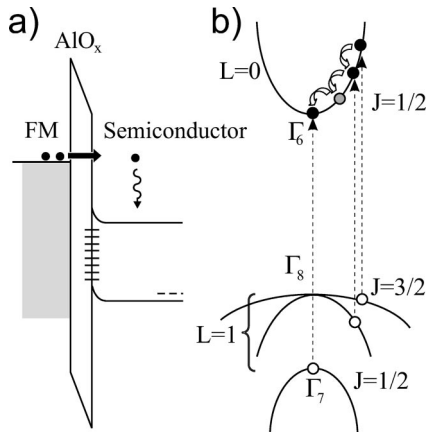


FIG. 6. Electrical injection of the hot electrons into a semiconductor schematically shown in a direct-space band scheme (a), and, depicted in k -space electron thermalization under optical excitation with $h \cdot \nu > E_g + \Delta$ (b).

partially lose their spin orientation during thermalization process, the net spin orientation on the bottom of the conduction band changes sign and becomes negative due to the contribution of “cold” electrons excited from the split-off valence band.^{32,7} Thus, by comparison of circular polarization of photoluminescence under excitation near the band gap E_g and slightly higher than $E_g + \Delta$, the spin loss during electron thermalization can be evaluated.

III. EXPERIMENTAL REALIZATION

A. Experimental setup

The experimental setup, shown in Fig. 7, allows measurements of the degree of circular polarization of the luminescence under electrical and optical excitation in an external oblique magnetic field. An optical cryostat allows cooling of the sample to about 80 K. The magnet provides an external oblique magnetic field up to 0.6 T.

The emitted light under electrical injection is coupled into an optical fiber by lens L_2 and is detected by a photodetector (PD₁). In this case we do not use any spectral filters, as EL spectra of our spin LEDs have shown GaAs interband transitions only (see Sec. III B).

For precise measurements of the degree of circular polarization of the emitted light we have used a combination of a rotating quarter-wave plate ($\lambda/4^*$) and linear polarizer (A) together with lock-in detection (locked to the double frequency of rotation of the quarter wave plate). For the case of optical spin injection and detection (all-optical experiment), semiconductor ($h\nu = 1.58$ eV) and He-Ne ($h\nu = 1.96$ eV) lasers (L) together with an optical monochromator and photodetector PD₂ are used.

B. Ferromagnetic metal/insulator/semiconductor spin LEDs

The studies of tunnel magnetoresistance (TMR) in metallic structures have shown that high efficiency of spin effects is generally achieved in systems with very abrupt interfaces,^{33,34} as the interdiffusion on interfaces leads to the formation of a so-called “dead layer” and a strong reduction

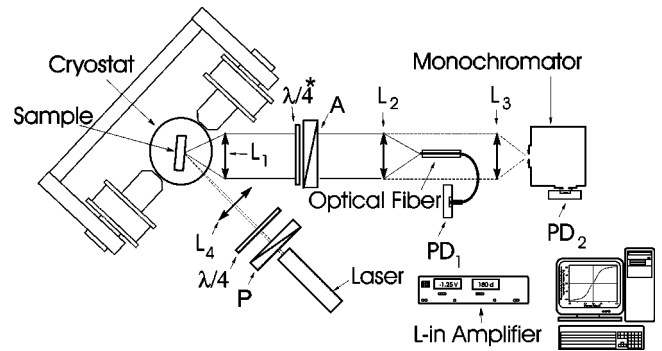


FIG. 7. Schematic representation of the setup for optical assessment of electrical and optical spin injection into semiconductors under external oblique magnetic field.

of the spin dependent effects. In the case of GaAs and other III-V compounds the abrupt metal/semiconductor junction leads to the Schottky barrier formation. The electron injection into the semiconductor conduction band is not so evident for the case of Schottky junctions. Let us consider the example of a metal/ p -type semiconductor Schottky junction [Fig. 8(a)]. The use of p -type semiconductor is preferable for optical assessment of electrical spin injection, as in n -type material the presence of strong background of unpolarized majority electrons complicates the quantitative determination of the injected spin polarization. The negative bias applied to the metallic contact of a ferromagnetic metal (FM)/ p -type semiconductor Schottky diode (forward bias) reduces the barrier on the semiconductor side of the junction and induces a strong hole current from the semiconductor into the metal (injection of electrons from the metal into the valence band). No electrons are injected into the semiconductor conduction band from the metal, since the barrier height on the metallic side of the junction is not reduced [Fig. 8(b)]. This can be remedied by introduction of a thin insulator (oxide) layer between the metal and the semiconductor. The drop of the potential across the tunnel junction reduces the energy separation between the Fermi level of the metal and the conduction band edge. At sufficiently high biases electrons can tunnel from the metal through the oxide layer directly into the conduction band. In addition, the negative bias applied to the metal leads to the formation of a hole accumulation layer at the semiconductor side of the junction, as a result practically all applied bias drops across the tunnel oxide layer.

In a real metal/insulator/semiconductor (MIS) tunnel junction, the application of the forward bias leads to the flow of three main currents [Fig. 8(c)]. Electrons tunneling from Fermi level of the metal into conduction band of the semiconductor, electrons tunneling from the metal into the valence band of the semiconductor (hole tunneling), and non-radiative recombination of the carriers via interface states. Only the first one results in spin injection and can be assessed optically. The two others do not reveal themselves in the optical output and result in local heating of the sample, higher stress (current, bias) applied to the tunnel oxide, device degradation, and unreliable operation. In order to reduce their contributions we introduce a thin undoped AlGaAs layer between the tunnel oxide and the GaAs [Fig. 8(d)]. It keeps the holes away from the oxide-semiconductor interface

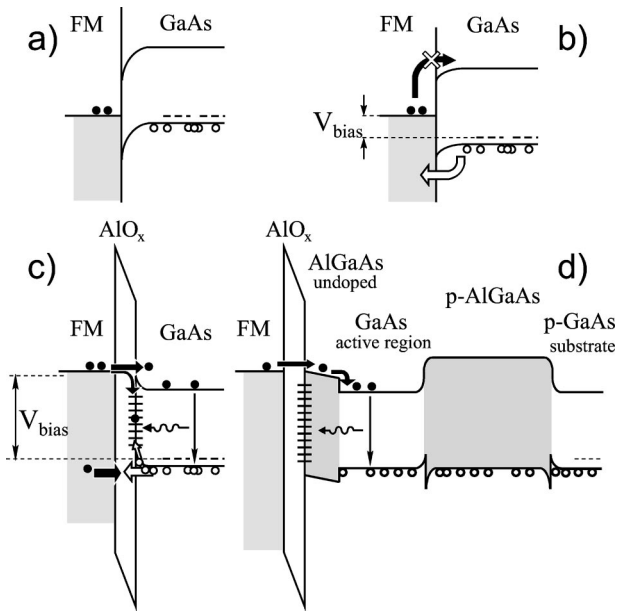


FIG. 8. Schematic representation of the spin-LED design. (a) and (b) FM/*p*-GaAs Schottky diode without and with applied bias: an efficient injection of electrons from the FM into the semiconductor is impossible. (c) In a MIS tunnel junction a moderate bias leads to a flow of three main currents in the heterostructure: from the FM Fermi level into the conduction band of the semiconductor, and from the FM into the valence band of the semiconductor (hole tunneling) and the surface recombination current. (d) Incorporation of the two AlGaAs layers leads to formation of the active region preserving GaAs bulk spin detection qualities.

and thus reduces the current through the interface states and the hole tunneling current to the metal. In order to enhance the radiative recombination efficiency, like in the conventional LED heterostructures, we introduce the second wide *p*-AlGaAs layer, which does not allow injected electrons to diffuse far from the surface. Two AlGaAs layers thus delimit the GaAs active region, where the injected electrons recombine with holes. In our devices, the active region is chosen to be wide enough such that no quantization of electron or hole levels takes place. We deliberately do not use the quantum wells in order to avoid complications related to the splitting of the valence band²³ and to the partial loss of the spin polarization during the electron trapping into the well, as it happens in quantum dots.³⁵ Thus the proposed FM/Insulator/Semiconductor spin-LEDs consist of two parts: the FM/AIO_x tunnel barrier (TB) spin injector and the III-V heterostructure spin detector. The initial experiments,^{25–28} have shown that very high efficiencies of spin injection can be achieved in these MIS heterostructures.

Two similar semiconductor heterostructures [Figs. 8(d) and 9, left] were grown by molecular beam epitaxy on a (001) *p*-GaAs substrate. Sample A: 2- μm *p*-GaAs buffer layer ($p = 2 \times 10^{18} \text{ cm}^{-3}$), 200-nm *p*-Al_{0.30}Ga_{0.70}As ($p = 2 \times 10^{18} \text{ cm}^{-3}$), 100-nm *p*-GaAs ($p = 2 \times 10^{18} \text{ cm}^{-3}$) active region and 15-nm Al_{0.20}Ga_{0.80}As (undoped). Sample B is an identical semiconductor heterostructure, the only difference is the GaAs active region is undoped.

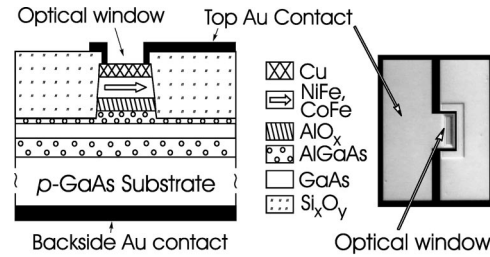


FIG. 9. Schematic representation of the fabricated MIS spin LEDs and the top view on the processed device, showing the top Au contact with an optical window.

After fabrication of the spin detector part of the spin LEDs, the samples were quickly transferred in air (the exposure to air was typically below 5–10 min) into the second vacuum chamber for fabrication of spin injectors. Where, on both types of semiconductor heterostructures identical FM/tunnel oxide spin injectors were fabricated using technology adopted from TMR junction fabrication process.³⁶ The thin AIO_x TB was fabricated by Al sputtering and subsequent natural oxidation in a controlled oxygen atmosphere of 140 Torr in a two-step process. In the first step, nominally 1-nm Al layer was sputtered and naturally oxidized. In the second step, a second 1-nm Al layer was deposited and naturally oxidized forming a thin 2.6-nm AIO_x TB. The use of a two-step oxidation process facilitates a full oxidation of the Al, reduces the chance on pinholes³⁷ and enables the fabrication of thicker barriers. This process results in an atomically flat, densely packed and pinhole free TBs.²⁸ After fabrication of the AIO_x TB, the 2-nm Co₉₀Fe₁₀/8-nm Ni₈₀Fe₂₀/5-nm Cu ferromagnetic stack was sputtered in the same vacuum chamber. All metals are dc-magnetron sputtered. Magnetic anisotropy was obtained by application of a small in-plane magnetic field of 4 mT.

After fabrication of the detector and injector parts of the devices, the surface emitting LEDs were processed using conventional optical lithography, dry and wet processing steps. Resulting in the $40 \times 120 \mu\text{m}^2$ magnetic rectangle contacts, with long side oriented along the easy axis of the FM magnetization. The devices were packaged and contacted using Au contacts to the backside of the substrate and to the FM, leaving an optical window (Fig. 9).

The easy magnetization axis of the ferromagnetic film is in-plane. The magneto-optical Kerr effect measurement shows a square hysteresis loop with coercivity of about 0.65 mT (Fig. 10). The effective saturation magnetization governing the out-of-plane tilting of the magnetization in our ferromagnetic film (see Sec. II B) is $\mu_0 \cdot M = 1.3 T$. It is determined from the extraordinary Hall effect measurements in a perpendicular applied magnetic field (Fig. 11).

Under application of forward bias, the LEDs emit light corresponding to the GaAs band gap transitions only (Fig. 12). At $\sim 80 \text{ K}$ the light emission threshold is around 1.7 V (Fig. 12, top insert) for both samples. In order to get sufficient signal to noise ratio, the measurements were carried out at 1.9...3.5 V bias and 30...100 mA current values. A typical result of I-V measurements is shown in Fig. 12 (lower inset).

The process of fabrication of the spin LEDs is quite reliable and gives very reproducible results. Until now more

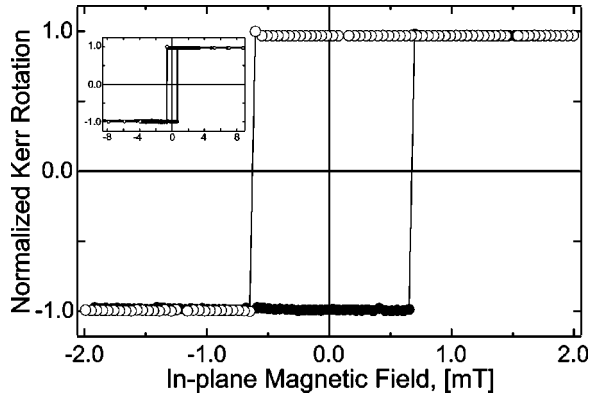


FIG. 10. Magneto-optical Kerr effect measurements of in-plane magnetic reversal. Inset: extended field range. The coercive field is 0.65 mT.

than ten fabrications starting from 2" GaAs wafer were performed. Each fabrication on the single wafer results in more than 100 spin-LEDs. All of the measured devices have shown similar characteristics.

IV. ELECTRICAL SPIN INJECTION INTO SEMICONDUCTORS

A. Electrical spin injection at 80 K

As it was mentioned before, our MIS spin LEDs can be considered to consist of two parts: the FM/ AlO_x TB-spin injector, and the III-V semiconductor heterostructure spin detector. In order to assess the spin injection in such heterostructure, the detector part of the junction has to be calibrated, which can be done in the all-optical experiment with optical spin injection and detection. Figure 13(a) shows a typical results of measurements of emitted circular polarization as a function of external oblique magnetic field under optical excitation with 100% circularly polarized light with $h \cdot \nu = 1.58$ eV ($h \cdot \nu \geq E_g$) and $h \cdot \nu = 1.96$ eV ($h \cdot \nu \geq E_g + \Delta$) for sample A (*p*-type active region). As discussed in the previous sections the optical measurements under excitation near the band gap of the semiconductor with 100% circularly polarized light allows complete characterization of the semiconductor as spin detector. The fitting of the data

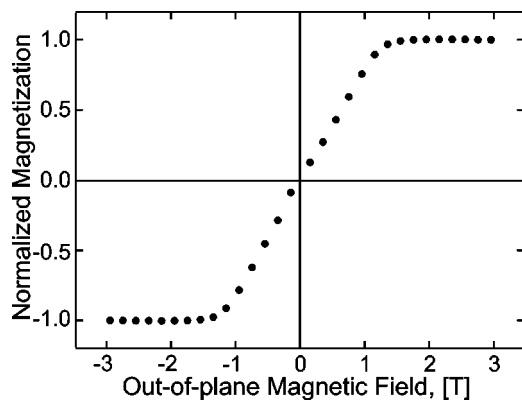


FIG. 11. Out-of-plane magnetization curve as revealed by extraordinary Hall effect measurements. The saturation field of 1.3 T is a measure for the saturation magnetization $\mu_0 \cdot M$.

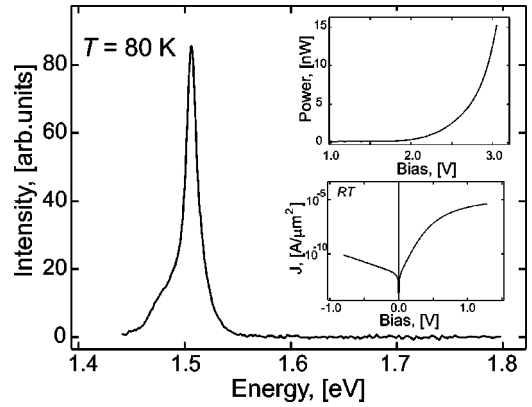


FIG. 12. Typical EL spectrum (sample B). Inset: optical output under forward bias and current density as function of applied bias of the MIS spin LEDs.

($h \cdot \nu = 1.58$ eV) with Eq. (2) [$S_0(0,0,1/4)$] reveals the following parameters of the GaAs active region: spin relaxation factor $T_s/\tau = 0.67 \pm 0.08$ and the half-width of the Hanle curve $\Delta B = (0.28 \pm 0.03)$ T. For excitation at $h \cdot \nu = 1.96$ eV, the reduced circular polarization is mostly due to excitation of electrons with opposite spin orientation from the split-off band. The measured *positive* value of the degree of circular polarization suggests that electrons do not lose their spin during the thermalization process (see Sec. II D).

In the same figure [Fig. 13(a)], we present the result of measurements of emitted circular polarization as a function of external oblique magnetic field under excitation with linearly polarized light $h \cdot \nu = 1.96$ eV, which does not create any spin polarization in the semiconductor.⁷ The observed polarization of the luminescence is due to the MCD effect in the ferromagnetic layer (see Sec. II C). It varies linearly with the magnetic field and gives the value of $D(B)$ which characterizes the MCD contribution to the observed circular polarization of light emitted by the structure. In order to obtain the real polarization of the emitted light P_{inj} we should subtract the D contribution from all measured P_{meas} values [see Eq. (10)]. Thus the subtraction of $D(B)$ from the curve $P_{meas}(B)$ [$h \cdot \nu = 1.96$ eV, Fig. 13(a)] transforms it into a perfect Lorentzian, typical for the Hanle effect. Note that the $D(B)$ is quite linear and changes sign when B passes through zero. As mentioned in Sec. III B, the ferromagnetic layer is made from a soft magnetic material, the hysteresis loop is quite narrow and is not seen on the scale of Fig. 13.

The typical result of measurements of circular polarization of the emitted light P_{meas} under application of electrical bias for sample A is shown in Fig. 13(b). The curve is non-linear with tendency to saturation at $B \geq 0.4$ T. The polarization changes sign when B passes through zero, which is related to the magnetization reversal in the FM. This clearly indicates that the observed polarization of luminescence is related to the ferromagnetic layer. The $P_{inj}(B)$ variation [Fig. 13(c)] is obtained from the measured curve by subtraction of $D(B)$ measured in the previous experiment.

As mentioned in Sec. II, $P_{inj}(B) = S_z(B)$ and we can fit the data of Fig. 13(c) using Eq. (6). The situation is quite different from the case of optical excitation near the GaAs band gap [Fig. 13(a)]. In the latter case S_0 is known (it is

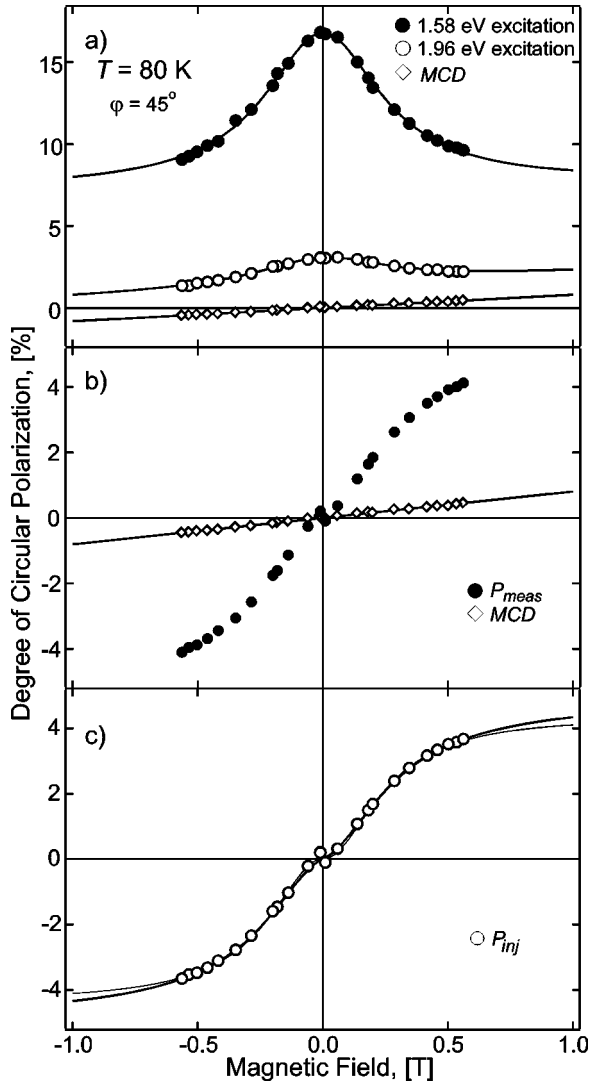


FIG. 13. Set of OHE measurements with optical and electrical spin injection for sample A (*p*-type active region). (a) Damping of the degree of circular polarization under optical spin injection with $h \cdot \nu = 1.58\text{ eV}$ and $h \cdot \nu = 1.96\text{ eV}$, Hanle fits using Eq. (2), and the MCD effect in the ferromagnetic film. (b) Typical result of a measurement of the degree of circular polarization of the electroluminescence, with the MCD contribution shown for comparison. (c) The change of circular polarization of the output of the device caused by the spin injection and precession only [the difference between spin injection and MCD curves in Fig. 13(b)], and Hanle fits using Eq. (4) (thin) and Eq. (6) (thick), from which the degree of injected spin polarization is determined: $\Pi = (21 \pm 3)\%$.

given by selection rules), the T_s/τ term is directly determined from the $P(B=0)$ value, the only fitting parameter remains the ΔB value. In the case of electrical spin injection, all three parameters should be obtained from the $P(B)$ variation: S_0 , T_s/τ , and ΔB . The first parameter is the most interesting one, since it characterizes the spin injection, i.e. the spin polarization of electrons injected from the FM into the semiconductor $\Pi = 2 \cdot S_0$. The last two parameters characterize the electron spin evolution in the active region of the MIS spin LED, i.e. they characterize the spin-detector part of our device. These parameters are known from the all-optical

calibration experiment [Fig. 13(a)], and the experimental data are perfectly fitted with the parameters T_s/τ and ΔB derived from these measurements. The thin line on the Fig. 13(c) is a fit made using Eq. (4) and the thick one using Eq. (6). These two fits give close values of spin injection: $\Pi = 26\%$ and $\Pi = 21\%$ excluding and including the effect of magnetization tilting in the FM, respectively.

Figure 14 represents results of measurements of circular polarization of the emitted light P_{meas} under application of electrical bias for two different orientations of the oblique magnetic field: $\varphi = 45^\circ$ and $\varphi = 60^\circ$ for sample A. The solid lines represent the fits obtained after Eq. (6) with the same set of parameters, the only difference is the oblique angle φ . (The curves were fitted independently, resulting in the same values of spin injection Π and half-width ΔB .) We want to emphasize here, that the angle dependence of the effect is perfectly described by Eq. (6).

Figure 15 shows the typical result of measurements of circular polarization of the emitted light $P_{inj}(B)$ (after MCD subtraction) under application of electrical bias for sample B (undoped active region). We do not have the results of the all-optical experiment for determination of spin detector parameters for this sample. This is because the undoped GaAs has very poor photoluminescence efficiency and it is difficult to discern this luminescence on the strong background of intense photoluminescence coming from highly *p*-doped substrate. The Hanle curve fit using Eq. (6) yields the following parameters: the injected spin polarization reduced by the spin scattering factor $\Pi \cdot T_s/\tau = (21 \pm 3)\%$ and the half-width of the Hanle curve $\Delta B = (0.16 \pm 0.02)\text{ T}$. The spin scattering parameter τ/T_s describes the spin scattering of electrons during their lifetime on the bottom of the conduction band of the semiconductor. Its value is not known for sample B, but in any case $\tau/T_s = (\tau_s + \tau)/\tau_s > 1$ and the real value of spin polarization of electrons injected through FM/semiconductor interface Π is certainly larger than 21%.

B. Room temperature measurements

Figure 16 shows the typical results of measurements of the circular polarization of the emitted light as a function of external oblique magnetic field ($\varphi = 45^\circ$) for sample A (doped active region). The data in Fig. 16(a) correspond to the optical excitations with the 100% circularly polarized light with $h \cdot \nu = 1.58\text{ eV}$. The fitting of the measured data after Eq. (2) reveals the following characteristic parameters of GaAs as a spin detector: spin relaxation parameter $T_s/\tau = 0.39 \pm 0.05$ and half-width of the Hanle curve $\Delta B = (0.8 \pm 0.1)\text{ T}$. These values differ significantly from the ones obtained at 80 K. The variation of these parameters is related to the enhancement of spin relaxation with temperature. This effect was studied in details in the 1970s.⁷ and our observations correspond quantitatively to the published data. At room temperature the half-width of the Hanle curve ΔB becomes very large, it is comparable to the magnetization saturation value of the ferromagnetic film $\mu_0 \cdot M$. As a result, the polarization of the electro-luminescence as a function of magnetic field does not show the typical Lorentzian shape. For the sample A, we can profit from the results of the all-

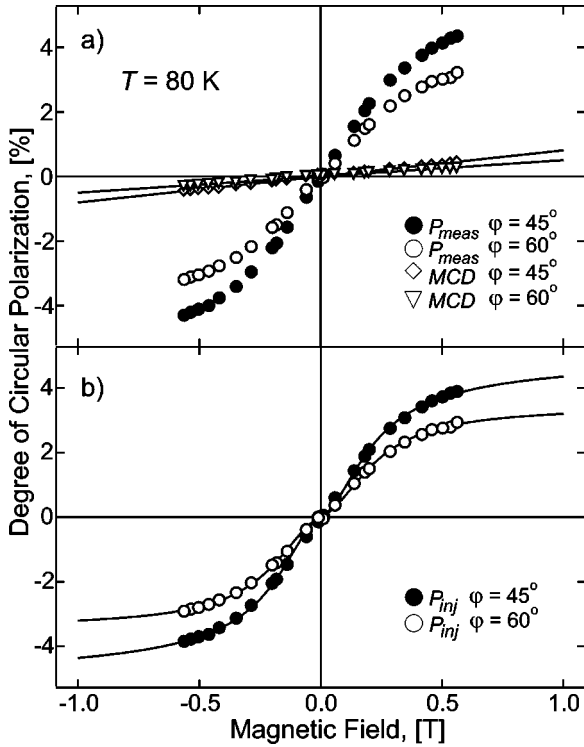


FIG. 14. Set of OHE measurements of electrical spin injection for sample A. (a) Measured degree of circular polarization of the electroluminescence in the external oblique magnetic field and MCD contributions. (b) The change of circular polarization of the optical output of the device caused by spin injection and precession only [the difference between spin injection and MCD curves in Fig. 14(a)], and Hanle fits [Eq. (6)] with the same sets of parameters: $\Pi = (21 \pm 3)\%$ and $\Delta B = (0.23 \pm 0.03)T$. The only difference is oblique angle ϕ .

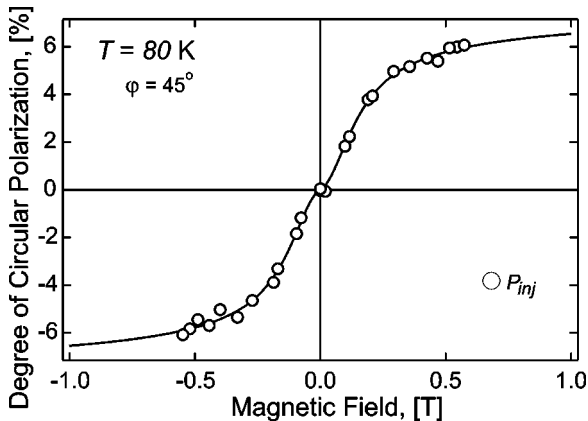


FIG. 15. Measurements for sample B (undoped active region) of the degree of circular polarization of the electroluminescence in the external oblique magnetic field after subtraction of the MCD contribution. The Hanle fit [Eq. (6)] reveals the injected spin polarization normalized to the spin scattering parameter $\Pi \cdot T_s / \tau = (21 \pm 3)\%$ and the half-width of the Hanle curve $\Delta B = (0.16 \pm 0.02)T$.

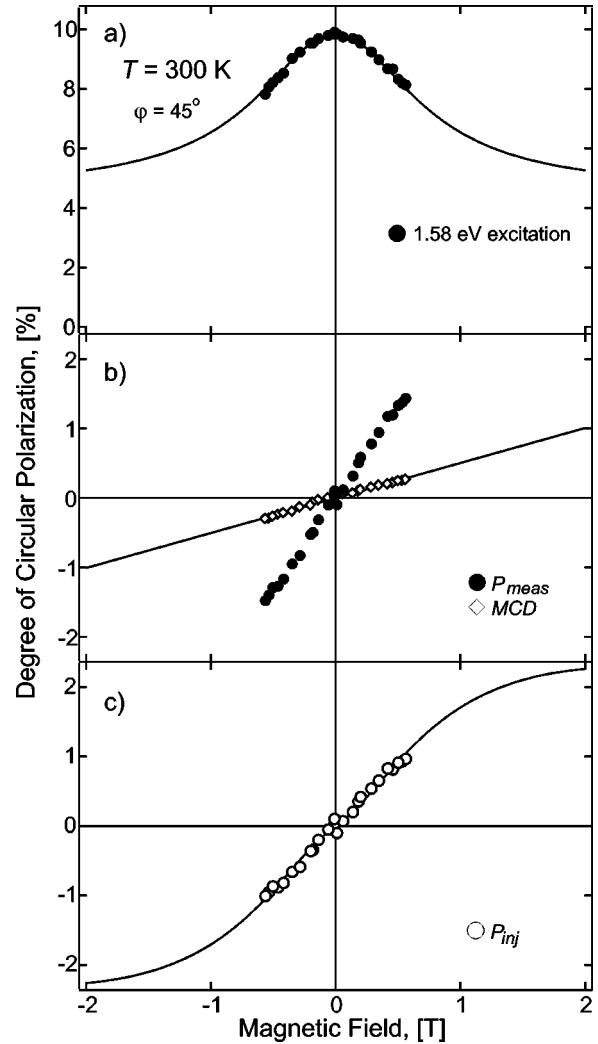


FIG. 16. Set of OHE measurements with optical and electrical spin injection for sample A (*p*-type active region). (a) Damping of the degree of circular polarization under optical spin injection with $h \cdot \nu = 1.58$ eV and the Hanle fit using Eq. (2). (b) Typical result of measurements of the degree of circular polarization of the electroluminescence and the MCD contribution. (c) The difference between spin injection and MCD curves in Fig. 16(b), and the Hanle fit using Eq. (6), from which the degree of injected spin polarization is inferred: $\Pi = (16 \pm 2)\%$.

optical experiment on determination of ΔB and T_s / τ values. The fitting of the measured data after subtraction of the MCD contribution $P_{inj}(B)$ [Fig. 16(c)] with these parameters [Eq. (6)] gives an injected spin polarization of $\Pi = (16 \pm 2)\%$.

Figure 17 shows for the sample B (undoped active region) the typical results of measurements of the circular polarization of the electroluminescence after subtraction of the MCD contribution $P_{inj}(B)$. As in the previous case, the saturation part of the Hanle curve is not reached in the available magnetic field range. However, the emitted light has substantially higher circular polarization than the MCD contribution. The Hanle fit after Eq. (6) reveals the following parameters, the minimal injected spin polarization normalized to spin scattering parameter $\Pi \geq (5 \pm 1) \cdot \tau / T_s \%$ and the minimal half-

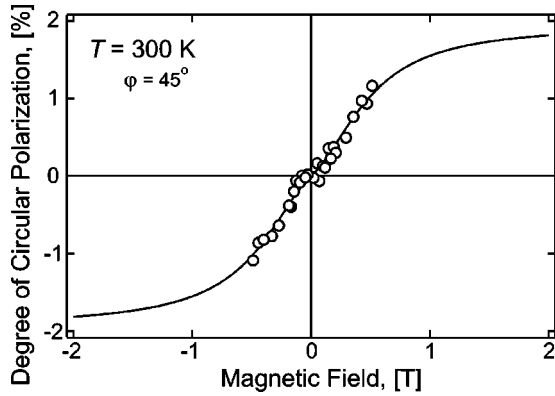


FIG. 17. Measurements for sample B (undoped active region) of the degree of circular polarization of the electroluminescence in the external oblique magnetic field after subtraction of MCD contribution. The Hanle fit [Eq. (6)] reveals the degree of injected spin polarization normalized to spin scattering parameter T_s/τ and $\Pi \cdot T_s/\tau \geq (5 \pm 1)\%$.

width of the Hanle curve $\Delta B \geq (0.6 \pm 0.2)$ T. Again the exact value of the spin scattering parameter T_s/τ is not known from independent measurements for sample B. A comparison of ΔB measured at low and room temperatures gives the following relative variation of T_s with temperature: $\Delta B_{300\text{K}}/\Delta B_{80\text{K}} \approx T_{s80\text{K}}/T_{s300\text{K}} \geq 3.8 \pm 1.3$ [see Eq. (3)]. Taking into account that the decrease of T_s is entirely due to enhancement of spin relaxation at room temperature (electron lifetime τ slightly increases while spin scattering time τ_s decreases drastically⁷):

$$\frac{T_s/\tau(300\text{ K})}{T_s/\tau(80\text{ K})} \leq \frac{T_s(300\text{ K})}{T_s(80\text{ K})} \Rightarrow$$

$$\tau/T_s(300\text{ K}) \geq \frac{T_s(80\text{ K})}{T_s(300\text{ K})} \cdot \tau/T_s(80\text{ K}).$$

Since the spin scattering term $\tau/T_s(80\text{ K}) = (\tau_s + \tau)/\tau_s > 1$, one can easily obtain a lowest limit of spin scattering term $\tau/T_s(300\text{ K}) > 3.8 \pm 1.3$ and injected spin polarization $\Pi \geq (19 \pm 7)\%$ at room temperature.

C. Influence of electrical bias

As our measurement technique allows simultaneous measurements of injected spin polarization and spin dynamics inside of the semiconductor (half-width of the Hanle curve), it is interesting to look how these parameters change as a function of the electrical bias applied to the device (devices are biased using electrical contacts to the FM and substrate; see Sec. III B). Figures 18 and 19 show typical bias dependencies observed for samples A and B, respectively at 80 K. For sample B with undoped active region, the measurements show quite strong reduction of the injected spin polarization with bias. For sample A with highly *p*-doped active region, the spin injection practically does not change with bias. (Here we can exclude any possibility of TB degradation or of its interfaces on the result of measurements, since experimental points were taken with increasing as well as decreasing bias sequence.) Such a behavior suggests that the effect

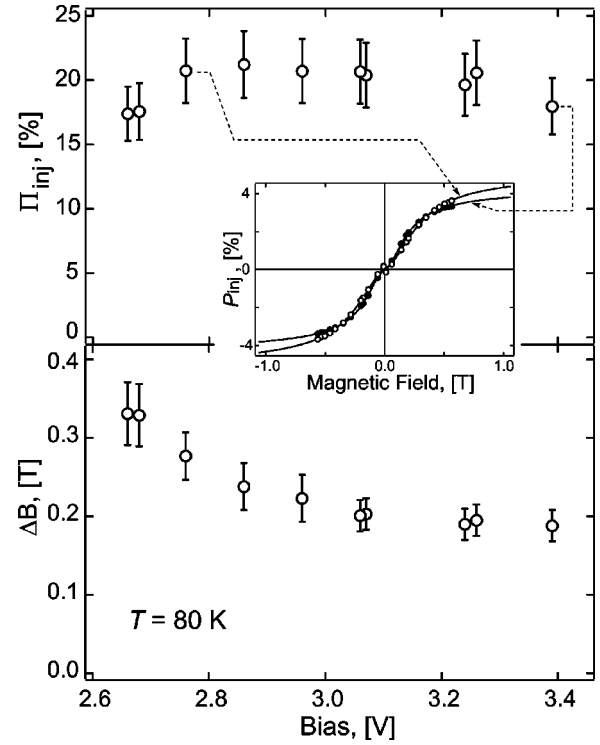


FIG. 18. Experimental bias dependencies of the injected spin polarization and the half-width of the Hanle curve for sample A (*p*-type active region).

is associated with properties of the active region of the device and not with the spin injection. The effect can be related to the loss of polarization during the thermalization of hot electrons. For higher biases the electrons injected into the active region have higher kinetic energy. From all-optical measurements it is known that the effect of spin scattering and loss of polarization during thermalization is much stronger in samples with lower doping level (Dyakonov-Perel mechanism⁷). This can explain the observed difference between samples A and B.

Another surprising fact is the narrowing of the Hanle curve with bias. At low bias the half-width of the Hanle curve corresponds to the one observed in all-optical measurements, and then decreases to lower values at higher biases. Even though this change is not very important (~ 1.5 times), so far it was observed on all measured devices on all fabricated samples. This change cannot be attributed to the heating of the sample at higher biases, when higher Joule energy is dissipated in the device. The heating causes the opposite effect—the acceleration of the spin relaxation and the increase of the half-width of Hanle curve ΔB .

The narrowing of the Hanle curve can also find an explanation in terms of thermalization process. If the thermalization is slow enough, the spin precession due to the external magnetic field during the thermalization cannot be neglected. As was observed in all-optical experiments, this leads to deformation and narrowing of the Hanle curve.³⁸ However, further investigation is needed for confirmation of this model.

Room temperature measurements have revealed similar tendencies for the bias dependencies of injected spin polarization. Within measurements error, no change of the half-

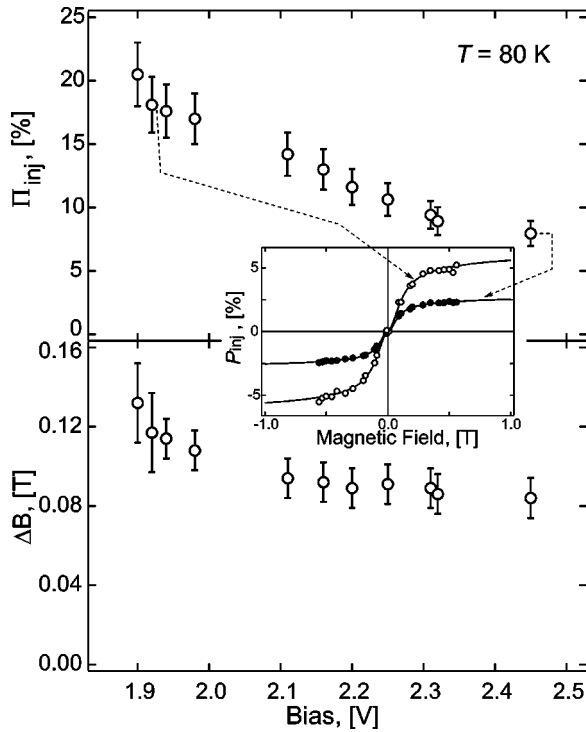


FIG. 19. Experimental bias dependencies of the injected spin polarization and the half-width of the Hanle curve for sample B (undoped active region).

width of the Hanle curve was observed at 300 K. This indicates that electron thermalization is fast and no spin precession occurs during this process.

D. TMR measurements

It is interesting to compare the spin polarization of electrons injected into the semiconductor with the electron spin polarization in the FM. In our case, the last one can be evaluated from TMR measurements.³⁹ Moreover it is known that the absolute value of the TMR effect depends not only on the absolute value of the spin polarization within the FM, but also on interface properties and the density of states within the tunnel barrier.^{40,41} The quality of the AlO_x interfaces and fabrication of the pinhole free tunnel barriers with good structural and electrical properties is of tremendous importance for both types of the devices. For this purpose, $\text{CoFe}/\text{AlO}_x/\text{CoFe}$ TMR junctions were repeatedly fabricated in the same sputtering system. These TMR junctions show 28% TMR effect at 80 K and 20% at 300 K. According to the Julliere theory⁴² these TMR values correspond to spin polarization in the FM of $\Pi=40\%$ and 30% at 80 and 300 K, respectively. The polarizations of injected electrons measured in our spin LEDs are already quite close to these values. We believe that spin injection in the hybrid ferromagnet/oxide/semiconductor devices can be improved the same way as in the TMR junctions, by improving the quality of the oxide barrier and its interfaces, and by using ferromagnetic materials with higher spin polarization.

V. CONCLUSIONS

The presented results show that the oblique Hanle effect approach represents a useful tool for optical assessment of electrical spin injection into semiconductors. It discriminates spin injection from side effects, e.g., magneto-optical and Zeeman splitting induced spin polarization. In addition, it provides very valuable information about spin kinetics within the semiconductor. Combined with all-optical characterization of the spin detector part of the device it represents a powerful tool for quantitative evaluation of the spin injection.

We also note that the electron spin relaxation time T_s , which defines the width of the Hanle curve in our experiments, is approximately of the same order in other common III-V compounds.^{43,44,7} In contrast, the g^* factors in these compounds strongly depend on the band structure parameters.⁴⁵ So for materials with higher g^* factors, for example GaSb [$g^*=9$ and 3 (Ref. 46)], the same value of spin scattering time T_s will give a much narrower (in the case of GaSb ~ 20 times narrower) Hanle curve. In this case, the Hanle measurements (even at room temperature) can be performed in very low external magnetic field, where the effect of tilting of magnetization in ferromagnetic film can be totally neglected.

To get a fast feedback on the quality of spin injectors used for spintronics applications it is very important to have an independent characterization tool. In our case the TMR junctions fabricated in the same sputtering system provide essential feedback on the quality of the ferromagnetic metal/tunnel barrier spin injectors. Moreover, such TMR data can be used to estimate the spin injection efficiency in the MIS-type heterostructures.

Our results indicate that the use of a tunnel barrier injector is indeed an interesting route to inject spins into a semiconductor. The introduction of an oxide layer allows one to fabricate more stable and robust spin injectors. A large variety of ferromagnetic materials can be deposited on top of the oxide layer, forming a universal spin source. We consider these to be very promising results for future room temperature spintronic devices using stable tunnel barrier injectors, such as Al_2O_3 or AlN on III-V (e.g., GaAs, GaN) or state-of-the-art SiO_2 for Si/SiGe devices.

ACKNOWLEDGMENTS

We thank Willem van de Graaf and Stefan Degroote for MBE growth, Jo Das for metal deposition and dry etch support, Liesbet Lagae for MOKE measurements, Mayke Nijboer for experimental assistance with development of the high quality AlO_x , and Reiner Windisch and Barun Dutta for experimental assistance and discussions. P.V.D. acknowledges financial support from the I.W.T. (Belgium). W.V.R. acknowledges financial support as a Postdoctoral Fellow of the Fund for Scientific Research Flanders-Belgium (F.W.O.). This work was supported in part by the EC Project No. SPINOSA (IST-2001-33334) and as an IMEC Innovation Project.

- *Also at Department of Physics, University of Antwerp-UIA, Belgium.
- †Also at Department of Electronic Engineering, K. U. Leuven, Belgium.
- ¹International Roadmap for Semiconductors, <http://public.itrs.net/>. Semiconductor Industry Association, <http://www.sia-online.org/>
- ²S. A. Wolf, D. D. Awschalom, R. A. Buhrman, J. M. Daughton, S. von Molnar, M. L. Roukes, A. Y. Chtchelkanova, and D. M. Treger, *Science* **294**, 1488 (2001).
- ³G. Burkard and D. Loss, *Europhys. News* **5**, 166 (2002).
- ⁴G. Prinz, *Science* **250**, 1092 (1990).
- ⁵G. Prinz, *Phys. Today* **48**(April), 58 (1995).
- ⁶Special Issue: Semiconductor spintronics, Guest Editor Hideo Ohno, *Semicond. Sci. Technol.* **17**, N4 (2002).
- ⁷M. I. D'yakonov and V. I. Perel', in *Optical Orientation*, edited by F. Meier and B. P. Zakharchenya (North Holland, Amsterdam, 1984), pp. 11–50.
- ⁸J. M. Kikkawa and D. D. Awschalom, *Phys. Rev. Lett.* **80**, 4313 (1998).
- ⁹R. I. Dzhiyev, B. P. Zakharchenya, V. L. Korenev, D. Gammon, and D. S. Katzer, *Pis'ma Zh. Eksp. Teor. Fiz.* **74**, 200 (2001) [*JETP Lett.* **74**, 182 (2001)].
- ¹⁰J. M. Kikkawa and D. D. Awschalom, *Nature (London)* **397**, 139 (1999).
- ¹¹D. Hagele, M. Oestreich, W. W. Ruhle, N. Nestle, and K. Eberl, *Appl. Phys. Lett.* **73**, 1580 (1998).
- ¹²I. Malajovich, J. J. Berry, N. Samarth, and D. D. Awschalom, *Nature (London)* **411**, 770 (2001).
- ¹³A. T. Filip, B. H. Hoving, F. J. Jedema, B. J. van Wees, B. Dutta, and S. Borghs, *Phys. Rev. B* **62**, 9996 (2000).
- ¹⁴G. Schmidt, D. Ferrand, L. W. Molenkamp, A. T. Filip, and B. J. van Wees, *Phys. Rev. B* **62**, R4790 (2000).
- ¹⁵E. I. Rashba, *Phys. Rev. B* **62**, R16267 (2000).
- ¹⁶E. I. Rashba, *Appl. Phys. Lett.* **80**, 2329 (2002).
- ¹⁷A. Fert and H. Jaffres, *Phys. Rev. B* **64**, 184420 (2001).
- ¹⁸R. Fiederling, M. Keim, G. Reuscher, W. Ossau, G. Schmidt, A. Waag, and L. W. Molenkamp, *Nature (London)* **402**, 787 (1999).
- ¹⁹Y. Ohno, D. K. Young, B. Beschoten, F. Matsukura, H. Ohno, and D. D. Awschalom, *Nature (London)* **402**, 790 (1999).
- ²⁰S. F. Alvarado and P. Renaud, *Phys. Rev. Lett.* **68**, 1387 (1992).
- ²¹V. P. LaBella, D. W. Bullock, Z. Ding, C. Emery, A. Venkatesan, W. F. Oliver, G. J. Salamo, P. M. Thibado, and M. Mortazavi, *Science* **292**, 1518 (2001).
- ²²A. T. Hanbicki, B. T. Jonker, G. Itskos, G. Kioseoglou, and A. Petrou, *Appl. Phys. Lett.* **80**, 1240 (2002).
- ²³H. J. Zhu, M. Ramsteiner, H. Kostial, M. Wassermeier, H. P. Schonherr, and K. H. Ploog, *Phys. Rev. Lett.* **87**, 016601 (2001).
- ²⁴B. L. Liu, M. Senes, S. Couderc, J. F. Bobo, X. Marie, T. Amand, C. Fontaine, and A. Arnoult, *Physica E* **17**, 358 (2003).
- ²⁵V. F. Motsnyi, V. I. Safarov, P. van Dorpe, J. Das, W. Van Roy, E. Goovaerts, G. Borghs, and J. De Boeck, *J. Superconductivity* **16**, 671 (2003) [cond-mat/0110240].
- ²⁶V. F. Motsnyi, V. I. Safarov, J. De Boeck, J. Das, W. Van Roy, E. Goovaerts, and G. Borghs, *Appl. Phys. Lett.* **81**, 265 (2002).
- ²⁷P. Van Dorpe, V. F. Motsnyi, M. Nijboer, E. Goovaerts, V. I. Safarov, J. Das, W. Van Roy, G. Borghs, and J. De Boeck, cond-mat/0208325 (unpublished).
- ²⁸P. Van Dorpe, V. F. Motsnyi, M. Nijboer, E. Goovaerts, V. I. Safarov, J. Das, W. Van Roy, G. Borghs, and J. De Boeck, *Jpn. J. Appl. Phys.* **42**, L502 (2003).
- ²⁹G. Lampel, *Phys. Rev. Lett.* **20**, 491 (1968).
- ³⁰M. I. D'yakonov, V. I. Perel', V. L. Berkovits, and V. I. Safarov, *Zh. Eksp. Teor. Fiz.* **67**, 1912 (1974) [*Sov. Phys. JETP* **40**, 950 (1975)].
- ³¹M. I. D'yakonov and V. I. Perel', *Fiz. Tverd. Tela (Leningrad)* **14**, 1452 (1972) [*Sov. Phys. Solid State* **14**, 1245 (1972)].
- ³²A. I. Ekimov and V. I. Safarov, *Pis'ma Zh. Eksp. Teor. Fiz.* **13**, 700 (1971) [*JETP Lett.* **13**, 495 (1971)].
- ³³S. Cardoso, P. P. Freitas, Z. G. Zhang, P. Wei, N. Barradas, and J. C. Soares, *J. Appl. Phys.* **89**, 6650 (2001).
- ³⁴U. Rudiger, R. Calarco, U. May, K. Samm, J. Hauch, H. Kittur, M. Sperlich, and G. Guntherodt, *J. Appl. Phys.* **89**, 7573 (2001).
- ³⁵V. K. Kalevich, M. Paillard, K. V. Kavokin, X. Marie, A. R. Kovsh, T. Amand, A. E. Zhukov, Yu. G. Musikhin, V. M. Ustinov, E. Vanelle, and B. P. Zakharchenya, *Phys. Rev. B* **64**, 045309 (2001).
- ³⁶H. Boeve, J. De Boeck, and G. Borghs, *J. Appl. Phys.* **89**, 482 (2001).
- ³⁷K. S. Moon, Y. Chen, and Y. Huai, *J. Appl. Phys.* **91**, 7965 (2002).
- ³⁸A. S. Volkov, A. I. Ekimov, S. A. Nikishin, V. I. Safarov, B. V. Tsarenkov, and G. V. Tsarenkov, *Pis'ma Zh. Eksp. Teor. Fiz.* **25**, 560 (1977) [*JETP Lett.* **25**, 526 (1978)].
- ³⁹I. I. Mazin, *Phys. Rev. Lett.* **83**, 1427 (1999).
- ⁴⁰J. M. De Teresa, A. Barthelemy, A. Fert, J. P. Contour, F. Montaigne, and P. Seneor, *Science* **286**, 507 (1999).
- ⁴¹J. Zhang and R. M. White, *J. Appl. Phys.* **83**, 6512 (1998).
- ⁴²M. Julliere, *Phys. Lett. A* **54**, 225 (1975).
- ⁴³V. I. Safarov and A. N. Titkov, *Proceedings of ICPS (International Conference on the Physics of Semiconductors), Kyoto* [*J. Phys. Soc. Jpn.* **49** (Suppl. A), 623 (1980)].
- ⁴⁴A. G. Aronov, G. E. Pikus, and A. N. Titkov, *Zh. Eksp. Teor. Phys.* **83**, 1170 (1983) [*Sov. Phys. JETP* **57**, 680 (1983)].
- ⁴⁵H. Kosaka, A. Kiselev, F. Baron, K. Kim, and E. Yablonoitch, *Electron. Lett.* **37**, 464 (2001), and references therein.
- ⁴⁶C. Hermann and G. Lampel, *Phys. Rev. Lett.* **27**, 373 (1971).